Constraints on perspective images and circular panoramas

Marc Menem* Tomáš Pajdla†
marc.menem@m4x.org pajdla@cmp.felk.cvut.cz
Center for Machine Perception, Department of Cybernetics,
Czech Technical University in Prague,
Karlovo nám. 13, 121 35 Prague, Czech Republic

Abstract

We describe an algebraic constraint on corresponding image points in a perspective image and a circular panorama and provide a method to estimate it from noisy image measurements. Studying this combination of cameras is a step forward in localization and recognition since a database of circular panoramas captures completely the appearance of objects and scenes, and perspective images are the simplest query images. The constraint gives a way to use a RANSAC-like algorithm for image matching. We introduce a general method to establish constraints between (non-central) images in the form of a bilinear function of the lifted coordinates of corresponding image points. We apply the method to obtain an algebraic constraint for a perspective image and a circular panorama. The algebraic constraints are interpreted geometrically and the constraints estimated from image data are used to auto-calibrate cameras and to compute a metric reconstruction of the scene observed. A synthetic experiment demonstrates that the proposed reconstruction method behaves favorably in presence of image noise. As a proof of concept, the constraints are estimated from real images of indoor scenes and used to reconstruct positions of cameras and to compute a metric reconstruction of the scene.

1 Introduction

A single panorama image contains more complete description of the object or place it represents than a perspective image thanks to its wide field of view and its ability to unfold objects. Therefore, a database of circular panoramas would be more representative with less data. It is also showed to produce less reconstruction error because its rays have a more favorable set of vergencies [14].

The ability to establish constraints between panoramas and perspective images is important when it comes to fetching a database of places or objects. Algebraic constraints are needed for automatic image search in a RANSAC-based matching algorithms [8, 7, 10].

*On the leave from Telecom Paris.

†This research was supported by BeNoGo IST-2001-39184, CONEX GZ 45.535, GACR 102/03/0440 and MSM 212300013 grants.

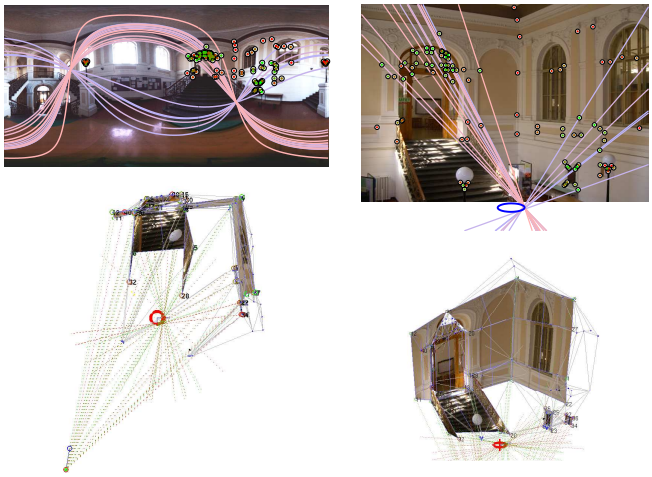

Figure 1: Constraints on corresponding points in a perspective image and a circular panorama can be formulated and used to establish correspondences, auto-calibrate the cameras, and compute a metric reconstruction of the scene.

This paper is the first step towards such an algorithm for other than perspective images. We show that constraints exist between perspective images and (non-perspective) circular panoramas and how they can be estimated from image data.

Circular panoramas have been used in image based rendering for their large field of view [12, 15]. The stereo geometry of a pair of circular panoramas has been studied [9, 5, 17] and geometric constraints between them were established [5, 4]. Reconstruction with a pair of un-calibrated central panoramas has been done from sparse [6, 1] as well as from dense correspondences [16]. All that previous work considered (often very special) combinations of circular panoramas.

In this work, circular panoramas are combined with perspective images. Combining different kinds of cameras was studied in a very general framework by [13]. Perspective images were previously combined by [18] with central catadioptric images. This works extends that to non-central panoramas. Our approach is in technicalities somewhat similar to the one used in [20, 2] for the X-Slits images.

2 Perspective Camera

The notations and the model for the perspective camera $P\mathbf{X} = \alpha\mathbf{x}, \alpha \in \mathbb{R} \setminus 0$, where P is a projection matrix, $\mathbf{X}$ is a scene point and $\mathbf{x}$ is its projection [3, page 139] follow the nomenclature used in [3]. We will use the decomposition of P in the form $P = \big(M \big| -M\mathbf{C}\big)$, where M is a 3×3 invertible matrix, and $\mathbf{C}$ is the *affine* center of the camera.

Given line coordinates $\mathbf{l}$ in the image, $P^\top\mathbf{l}$ are world coordinates of the plane π projecting to $\mathbf{l}$. Since all rays of the camera pass through $\mathbf{C}$, we have $\mathbf{C} \in \pi$ [3, page 186]. For a point $\overline{\mathbf{x}}$ in the image, $[\overline{\mathbf{x}}]_\times$ [3, page 554] is a rank two system of three lines passing through point $\overline{\mathbf{x}}$. We thus have the rank two system $[\overline{\mathbf{x}}]_\times P$ of three planes passing through image point $\overline{\mathbf{x}}$, and center of projection $\mathbf{C}$. At least two of the planes of $[\overline{\mathbf{x}}]_\times P$ are lin-

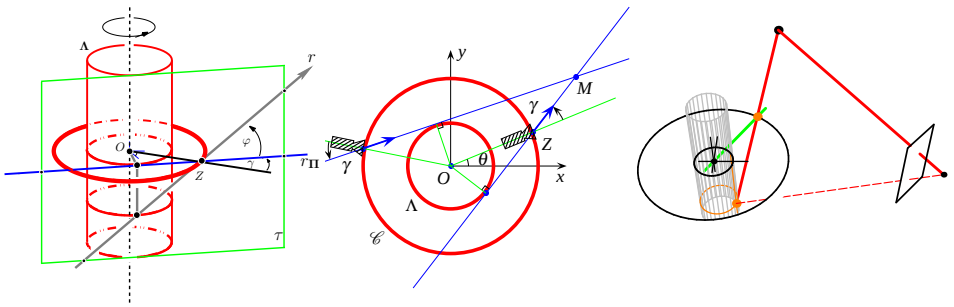

Figure 2: **2(a)** With a circular camera, point M is captured by a ray secant to the circular path $\mathscr{C}$, and tangent to the cylinder Λ. **2(b)** Points outside Λ have two images and points inside Λ have no image. **2(c)** Rays intersecting a point in space are coplanar. The constraint on corresponding image points $\overline{\mathbf{x}}^\top \mathsf{Q}\, \mathbf{x} = 0$ can be interpreted geometrically.

early independent, and their intersection is the ray $\overline{r}$ forming image point $\overline{\mathbf{x}}$. We need to intersect two linearly independent planes to obtain dual Plücker coordinates of $\overline{r}$, so we form the rank 1 system of matrices $L_{ij} = \mathbf{L}_i \mathbf{L}_j^\top - \mathbf{L}_j \mathbf{L}_i^\top$ where L_i is a line of $[\overline{\mathbf{x}}]_\times P$ and $(i,j) \in \{1,2,3\}^2, i \neq j$, and look for its span. We get a skew-symmetric matrix $\overline{L}$ which is the dual Plücker coordinates of $\overline{r}$.

3 Circular panoramas

Consider a sequence of images acquired by a perspective camera rotating along a circular path $\mathscr{C}$ around the center $\mathbf{O}$ and contained in a plane π. A *circular panorama* is the mosaic obtained by stitching side by side the same column taken from all images of the sequence (figure 2(b)) [1, 16]. The two parameters of the setup are the radius R of circle $\mathscr{C}$ and the angle of view γ corresponding to the column which is sampled.

We will be considering the case when the perspective camera can capture a complete pencil of rays in the plane defined by its angle γ. In practice, this is obtained by using a panoramic fisheye lens and shooting the sequence twice with the camera facing opposite directions or by sampling the 180° circle [17]. The rays of the circular panorama do not all intersect in a single point but they all intersect $\mathscr{C}$.

3.1 Properties of a circular panorama

The rays of a circular panorama are indexed by angle θ, indicating the position of their intersection with circle $\mathscr{C}$, (figure 2(b)) and angle φ indicating their elevation from the plane π (figure 2(a)). The image has the topology of a torus around $\mathscr{C}$.

Consider a ray r (figure 2(a)). Denote the intersection of r with $\mathscr{C}$ by $\mathbf{Z}$, and the projection of r to the plane π by r_π. By construction, r_π contains angle γ with line $\mathbf{OZ}$. If we build the cylinder Λ, centered in $\mathbf{O}$ and tangent to r_π, the radius of Λ is $R\sin\gamma$ (figure 2(b)). The radius does not depend on the ray r, only on the parameters of the camera. All the rays are tangent to Λ. Since it is possible to draw two different tangents to Λ from a

point $\mathbf{X}$ outside Λ, the point $\mathbf{X}$ has two images. It is not possible to draw a tangent to Λ from a point $\mathbf{X}$ inside Λ. Thus, such point $\mathbf{X}$ has no image.

3.2 Coordinates of a ray for a circular camera

Let us now work in a Cartesian coordinate system centered in the center of the circle $\mathscr{C}$ and with the z axis perpendicular to plane π. Coordinates of the intersection point $\mathbf{Z}$ of the ray r with the circle $\mathscr{C}$ and coordinates of the intersection point $\mathbf{Z}_\infty$ of r with the plane at infinity can be written, using image coordinates θ and φ, as $\mathbf{Z} = (R\cos\theta, R\sin\theta, 0, 1)^\top$ and $\mathbf{Z}_\infty = (\cos(\theta+\gamma)\cos\varphi, \sin(\theta+\gamma)\cos\varphi, \sin\varphi, 0)^\top$ respectively. Since the path of the circular camera is in affine space, it can be assumed that point $\mathbf{C}$ will never be at infinity. Plücker coordinates of r are obtained as $L = \mathbf{Z}\mathbf{Z}_\infty{}^\top - \mathbf{Z}_\infty\mathbf{Z}^\top$.

The simplicity of the circular panorama is the consequence of the fact that the coordinates of the ray can be obtained easily from and the image coordinates (θ, φ) and only *two* calibration parameters.

4 Constraints on two views

We derive a constraint in the form $\bar{\mathbf{x}}^\top \mathsf{Q}\,\mathbf{x} = 0$ where $\bar{\mathbf{x}}$ are the coordinates of a point in the perspective image, and $\mathbf{x}$ are the lifted coordinates of the corresponding point in the circular panorama. While such a constraint can always be found in two-views geometry if the rays intersect, the situation presented here is unique, because the circular camera has only two calibration parameters. Matrix Q can be decomposed to separate perspective and circular camera calibration. It is therefore easy to project $\tilde{\mathsf{Q}}$, estimated from noisy data, into the space of admissible matrices Q.

4.1 Deriving the fundamental matrix Q

Let r and $\bar{r}$ be projection rays of a pair of corresponding points in the circular panorama and in the perspective image respectively. Let $\bar{\mathscr{L}}^*(\bar{r}) = (\bar{l}^*_{12}, \bar{l}^*_{34}, \bar{l}^*_{13}, \bar{l}^*_{42}, \bar{l}^*_{14}, \bar{l}^*_{23})^\top$ denote the dual Plücker coordinates of $\bar{r}$. Similarly, let $\mathscr{L}(r) = (l_{12}, l_{34}, l_{13}, l_{42}, l_{14}, l_{23})^\top$ denote Plücker coordinates of r. Rays r and $\bar{r}$ intersect in a point and therefore are coplanar. Lines $\bar{\mathscr{L}}$ and $\mathscr{L}$ are coplanar iff the six-vector dot product of $\bar{\mathscr{L}}^*$ and $\mathscr{L}$ vanishes [3, page 54]

$$\bar{\mathscr{L}}\,\bar{\mathscr{L}}^* = l_{12}\bar{l}^*_{12} + l_{34}\bar{l}^*_{34} + l_{13}\bar{l}^*_{13} + l_{42}\bar{l}^*_{42} + l_{14}\bar{l}^*_{14} + l_{23}\bar{l}^*_{23} = 0. \tag{1}$$

We shall represent a perspective, resp. a circular, image point as $\bar{\mathbf{x}} = (x,\ y,\ w)^\top$, resp. $\mathbf{x} = (\cos(\varphi),\ \cos(\varphi)\cos(\theta),\ \cos(\varphi)\sin(\theta),\ \sin(\varphi),\ \sin(\varphi)\cos(\theta),\ \sin(\varphi)\sin(\theta))^\top$, where $\bar{\mathbf{x}}$ are homogeneous coordinates of a point in a projective plane and *lifted coordinates* $\mathbf{x}$ are

$$\mathsf{G} = \begin{pmatrix} -m_{31} & m_{21} & m_{31}y_c - m_{21}z_c & -m_{11} & m_{31}x_c - m_{11}z_c & m_{21}x_c - m_{11}y_c \\ -m_{32} & m_{22} & m_{32}y_c - m_{22}z_c & -m_{12} & m_{32}x_c - m_{12}z_c & m_{22}x_c - m_{12}y_c \\ -m_{33} & m_{23} & m_{33}y_c - m_{23}z_c & -m_{13} & m_{33}x_c - m_{13}z_c & m_{23}x_c - m_{13}y_c \end{pmatrix} \quad \mathsf{T} = \begin{pmatrix} R\sin\gamma & 0 & 0 & 0 & 0 & 0 \\ 0 & 0 & 0 & 0 & R & 0 \\ 0 & -\cos\gamma & 0 & \sin\gamma & 0 & 0 \\ 0 & 0 & 0 & 0 & 0 & R \\ 0 & \sin\gamma & 0 & \cos\gamma & 0 & 0 \\ 0 & 0 & -1 & 0 & 0 & 0 \end{pmatrix}$$

$(m_{ij}) = (M)^{-1}$, and $\mathbf{C} = (x_c, y_c, z_c)^\top$ are the parameters of the perspective camera.

a function of circular panorama coordinates (θ, φ). Plücker coordinates of the corresponding rays can be written as $\mathscr{L}^*(\bar{r}) = \mathsf{G}^\top \bar{\mathbf{x}}$ and $\mathscr{L}(r) = \mathsf{T}\mathbf{x}$. G and T are given on the bottom of page 4.

Let us consider a circular panorama. An image point (θ, φ) is mapped to a ray r. Lifted coordinates $\mathbf{x}$ of r are related to the interpretation of Plücker coordinates of r as a reordering of the coordinates of a direction vector of r and a vector orthogonal to r. The product of $\mathbf{x}$ with matrix T transforms the two orthogonal vectors, which depend on image coordinates (θ, φ), to the Plücker coordinates of r. Parameter γ rotates the direction vector around the z axis (and rotates and scales the other vector to stay orthogonal), and parameter R changes the distance of the intersection of r with plane π to the origin by scaling the other vector.

Matrices G and T are constant for a given setup of two cameras. Matrix G depends only on parameters of the perspective camera and matrix T depends only on parameters of the circular camera. The expected algebraic constraint on the coordinates of corresponding image points is obtained by substituting the above to (1) as

$$\bar{\mathbf{x}}^\top \mathsf{Q}\, \mathbf{x} = 0, \qquad \text{with} \quad \mathsf{Q} = \mathsf{G}\, \mathsf{T}. \tag{2}$$

Note that in the special case when $R = 0$, the circular camera is equivalent to a central spherical camera, and matrix Q becomes a 3×3 matrix.

4.2 Search curves

The relation (2) implies a constraint on corresponding image points. The locus of points verifying equation (2) can be found by solving equation $\bar{\mathbf{x}}^\top \mathsf{Q}\, \mathbf{x} = 0$ for a given point $\mathbf{x}_0$ (resp. $\bar{\mathbf{x}}_0$) and unknown $\bar{\mathbf{x}}$ (resp. $\mathbf{x}$). We get equations of a search curve

$$\bar{\mathbf{x}}^\top \mathsf{Q}\, \mathbf{x}_0 = 0, \quad \text{resp.} \quad \bar{\mathbf{x}}_0^\top \mathsf{Q}\, \mathbf{x} = 0, \tag{3}$$

in the perspective, resp. circular, image. Using the notation $\bar{\mathbf{x}}_0^\top \mathsf{Q} = (a_0, b_0, c_0, d_0, e_0, f_0)$, we get the equation of the search curve in the circular panorama

$$\begin{aligned} a_0 \cos(\varphi) + b_0 \cos(\varphi)\cos(\theta) + c_0 \cos(\varphi)\sin(\theta) \\ + d_0 \sin(\varphi) + e_0 \sin(\varphi)\cos(\theta) + f_0 \sin(\varphi)\sin(\theta) = 0 \end{aligned}$$

and finally

$$\tan(\varphi) = -\frac{(d_0 + e_0 \cos(\theta) + f_0 \sin(\theta))}{(a_0 + b_0 \cos(\theta) + c_0 \sin(\theta))}. \tag{4}$$

Equation (4) has two solutions for every value of φ. Thus, for one perspective image point $\bar{\mathbf{x}}$, we get two curves in the circular panorama.

The search curve can be interpreted geometrically. The image $\mathbf{x}$ (resp. $\bar{\mathbf{x}}$) of a point $\mathbf{X}$ is mapped to a ray r (resp. $\bar{r}$) (figure 2(c)). The locus of the corresponding points $\bar{\mathbf{x}}$ (resp $\mathbf{x}$) in the other image is the image of r (resp $\bar{r}$). Since writing the fundamental relation $\bar{\mathbf{x}}^\top \mathsf{Q}\, \mathbf{x} = 0$ induces loss of orientation information [21], the search curve (4) obtained from Q is a superset of the image of a line. The curve (4) is not a correspondence curve, since some of its points are not possible correspondences [11].

4.3 Decomposing Q into parameters

Matrix Q depends only on six parameters $\gamma, R, \det(M), x_c, y_c$ and z_c. Given an admissible Q, the parameters can be computed by writing down the system of equations involving the 18 non-zero subdeterminants out of the total number of 20 3×3 subdeterminants of Q

$$\begin{aligned} -\det(M)\, R\, x_c^2\, \sin\gamma &= \det \mathsf{Q}_{456} \\ -\det(M)\, R\, z_c\, \sin\gamma\,(-y_c\cos\gamma + x_c\sin\gamma) &= \det \mathsf{Q}_{356} \\ \vdots \quad\quad \vdots \quad\quad \vdots & \\ -\det(M)\, R^2\,(x_c\cos\gamma + y_c\sin\gamma) &= \det \mathsf{Q}_{124} \\ 0 &= \det \mathsf{Q}_{123}, \end{aligned} \tag{5}$$

where subscript ijk of Q_{ijk} denotes the columns that are left out from Q to form a 3×3 minor. R can be fixed as the scale parameter of the problem, e.g. to one, and the modified system can be solved for $\gamma, \det(M), x_c, y_c$ and z_c.

There are more equations in (5) than unknowns, and thus there are more ways how to compute unknowns. A choice of a five-tuple of equations out from (5) gives a particular solution. If Q is admissible, all choices that give a solution, give the same solution. If Q is not admissible, the solutions are in general different for different choices. By choosing one of them (or any function of them), a particular projection of inadmissible Q to the space of the admissible ones is done.

It seems to be the property of common circular panorama-perspective camera systems that any choice gives a reasonable initial estimate of the admissible Q. This is not true in general and allowed us to proceed farther here than with two X-Slits cameras in [2].

5 Calibrating the system

Q can be estimated from point correspondences using an adapted version of the classical Singular Value Decomposition algorithm:

1. For each pair of corresponding points $\mathbf{x}_i \leftrightarrow \bar{\mathbf{x}}_i$, $\bar{\mathbf{x}}_i^\top \tilde{\mathsf{Q}}\ \mathbf{x}_i = 0$ is re-written as the product of vectors $A_i\ q = 0$, where q contains values of $\tilde{\mathsf{Q}}$ and elements of A_i are products of coordinates.
2. Matrix $A = [A_1; A_2; \cdots]$ is filled with vectors A_i for each correspondence
$$A = \begin{pmatrix} u_0\cos\varphi_0 & u_0\cos\varphi_0\cos\theta_0 & \cdots \\ u_1\cos\varphi_1 & u_1\cos\varphi_1\cos\theta_1 & \cdots \\ \vdots & \ddots & \end{pmatrix}$$
3. According to the method described in [3, page 265], the rows of matrix A are all scaled to have norm one.
4. SVD is used to find $\ker A$, which is equivalent to solving for q in $A\ q = 0$.
5. Use method described in 4.3 to extract an initial guess of the calibration parameters: γ, the center of the perspective camera (x_c, y_c, z_c).
6. Use γ and $R = 1$ to compute T. Then compute T^{-1} and $\tilde{\mathsf{G}} = \tilde{\mathsf{Q}}\ \mathsf{T}^{-1}$

7. Read values of M^{-1} directly from $\tilde{\mathsf{G}}$ and compose P. Recompose Q.

Since only linear methods were used, the estimated $\tilde{\mathsf{Q}}$ at step 4 does not satisfy the constraints to fit in the form (2). The estimate is almost never accurate enough to be used for reconstruction. Therefore, $\tilde{\mathsf{Q}}$ is to be projected to the space of matrices Q's satisfying (2) by using the reprojection described in section 4.3.

A bundle adjustment allows to refine the estimation of the parameters used to compute Q by minimizing non-linearly the reprojection error. Assuming that the noise in correspondences has an identical independent normal distribution, the likelihood of Q is maximized. We use the Matlab function `lsqnonlin`, which implements the Levenberg-Marquardt algorithm, to minimize

$$\varepsilon(R,\gamma,P) = \sum_{i=1}^{n} \mathrm{d}^2(\mathbf{x}_n, l_n) + \mathrm{d}^2(\bar{\mathbf{x}}_n, \bar{l_n}),$$

where $\mathrm{d}(\mathbf{x}_\mathrm{n}, \mathrm{l}_\mathrm{n})$ is the Euclidean distance of an image point from its associated search curve.

6 Experiments

Several tests were run on simulated data in order to evaluate the performance of the algorithm. Let us first describe the protocol. We drew 100 3D points from a Gaussian distribution because this is the number of points we manually selected for the real data experiments. The perspective camera was chosen so that image data would be typically in range of $[-0.5, 0.5]$. The circular panorama data is chosen with $\gamma = \pi/12$ – note that this parameter does not seem to have an influence on the algorithm – and the distribution of image data falls in two intervals of length 1 (see figure 3). The algorithms presented in this paper were then used to calibrate the system and a metric reconstruction was obtained with the method described in [3, page 297].

For figure 3, a gaussian noise of variance 10^{-3} was added to both images. That is equivalent to error 0.1% of image size, i.e. 0.5 pixel in a 500×500 image. We present the reconstruction (figure 3(a)), the circular panorama with some of the search curves (figure 3(b)), and the perspective image with the corresponding search curve in the same colour (figure 3(c) and figure 3(d)), with the image of the circular camera in blue. Note that on figure 3(a) only one pair of cameras is visible because the reconstructed cameras are indistinguishable from the real ones

The curves of figure 3 show the variance of the distance of reconstructed points to their real positions for different levels of added noise to the image data. The noise levels considered range from 0 to 10^{-2}, and logarithmic scales were used for both axis. Different curves have been used to represent a different level of noise on the circular panorama, while the abscissa have been used to represent the level of noise on the perspective image. Angle γ is estimated with 1.51° error.

The observation from this experiment is that the noise in one image is completely masked by the noise in the other until some level. For a given noise level in the circular panorama, the reconstruction error is constant while the noise on the perspective image is below some value. It is thus possible to predict the reconstruction error based on the input noise.

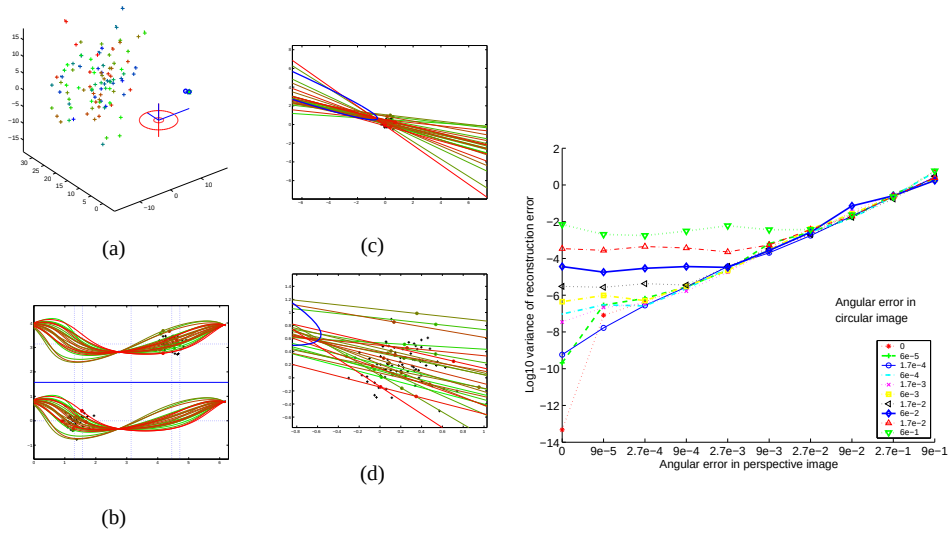

Figure 3: Simulated data experimental setup. 3(a) reconstructed points and cameras. 3(b) circular panorama with some search curves 3(c) Perspective image with the image of the reconstructed camera, and some search curves 3(d) Detail of the perspective image. The search curves and the corresponding points are drawn in the same colour. Variance of the distance of reconstructed points to their true position for different levels of added noise. The different curves are for different values of added noise to the circular panorama data, ranging from 0 to 10^{-2}. Variance of noise added to the perspective image is on the horizontal axis. Notice that for equivalent noise on both images this variance is a linear function of the added noise.

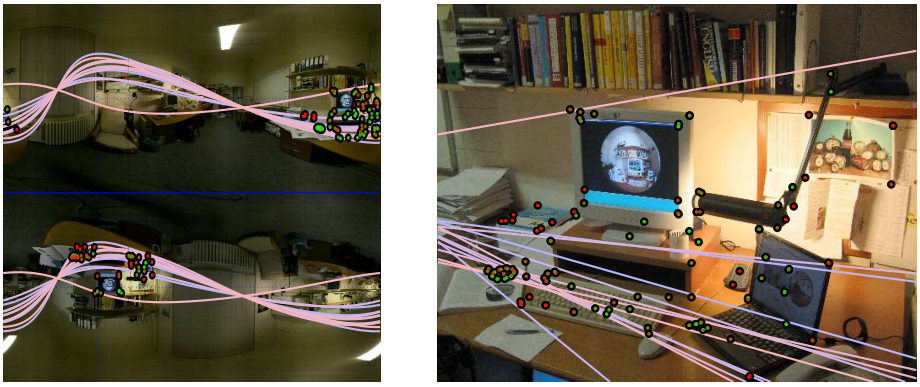

Figure 4: The non-centrality of the circular panorama is very strong in these images since the desk was very close to the circular camera.

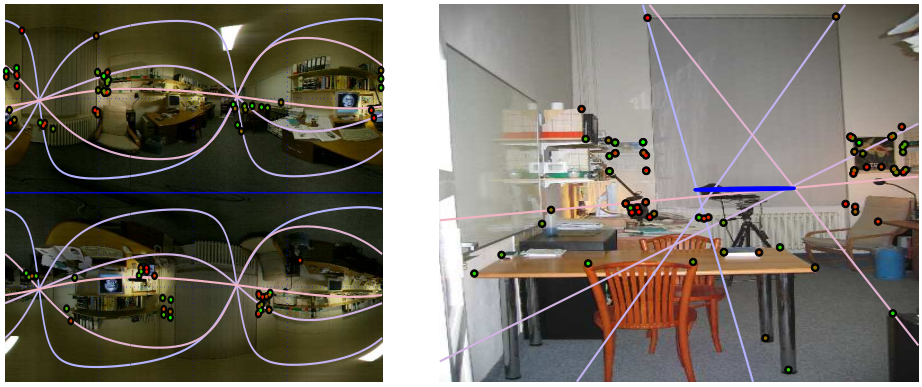

Figure 5: These two images show how the calibration process can reconstruct the circular camera. The perspective image was taken during the acquisition of the circular panorama. Notice the tripod and the black line segment that corresponds to the projection of the circular path of the camera into the perspective image.

6.1 Real data

In figure 1, the circular panorama was built from a sequence taken with a fisheye camera, so it has a field of view of $360^\circ \times 180^\circ$ it has a full resolution of 2200×1100 pixels; the perspective image was taken by a regular $4M$ pixel camera. 100 correspondences were established manually, and were used to calibrate the system. After bundle adjustment, the calibration parameters were used to reconstruct a scene model. For visualization purposes, textures have been mapped to the model from the perspective image. Metric reconstruction is possible because the image used is already calibrated and we have access to angles directly from the data.

Figure 4 and figure 5 show calibration of two $4M$ pixel views of an office against a circular $360^\circ \times 360^\circ$ circular panorama of resolution 5300×5300 pixels. The circular panorama was built by sampling the 180° circle of a a sequence of fisheye images. The angle γ used to build it was 180°.

In figure 4, the circular camera was very close to the desk, the circular panorama is thus very distorted. The non-central model accounts for this distortion. The reconstruction (figure 4) shows some objects of the scene and the circular camera, and on the calibrated image, the search curves all intersect twice in a point where the perspective image was taken. The angle γ was estimated with a 1.51° error.

In figure 5, we can verify that the circular camera is reconstructed correctly, since the tripod used for acquisition of the circular panorama is present in the scene. This calibration is also good because the search curves cross in the doorway, where the perspective image was taken. This scene contains objects on all sides of the circular camera, and the positions of the search curves on the perspective image show the position of the circular camera acquiring this point. The angle γ was estimated with a 0.21° error.

References

[1] H. Bakstein and T. Pajdla. 3D reconstruction from 360 x 360 mosaics. In *CVPR*, volume 2, pages 72–77. IEEE Computer Society, December 2001.

[2] D. Feldman, T. Pajdla, and D. Weinshall. On the epipolar geometry of the crossed-slits projection. In *ICCV 2003*, volume 2, pages 988–995. IEEE Computer Society, October 2003.

[3] R. Hartley and A. Zisserman. *Multiple View Geometry in Computer Vision*. Cambridge University Press, 2000.

[4] F. Huang and T. Pajdla. Epipolar geometry in concentric panoramas. Technical Report CTU-CMP-2000-07, Center for Machine Perception, 2000.

[5] F. Huang, S. K. Wei, and R. Klette. Geometrical fundamentals of polycentric panoramas. In *ICCV*, volume 1, pages 560–565. IEEE Computer Society, July 2001.

[6] S. B. Kang and R. Szeliski. 3-D scene data recovery using omnidirectional multibaseline stereo. *IJCV*, 25(2), Nov. 1997.

[7] D. Lowe. Local feature view clustering for 3D object recognition. In *CVPR 2001*, pages 682–688.

[8] J. Matas, O. Chum, M. Urban, and T. Pajdla. Robust wide baseline stereo from maximally stable extremal regions. In *BMVC 2002*, volume 1, pages 384–393, 2002.

[9] McMillan and Bischop. Plenoptic modeling: An image-based rendering system. In *SIGGRAPH 95*.

[10] K. Mikolajczyk and C. Schmid. A performance evaluation of local descriptors. In *CVPR*, volume 2, pages 257– 263, 2003.

[11] T. Pajdla. Epipolar geometry of some non-classical cameras. In *CVWW*, pages 223–233. Slovenian Pattern Recorgnition Society, February 2001.

[12] S. Peleg and M. Ban-Ezra. Stereo panorama with a single camera. In *CVPR 1999*, pages 395–401.

[13] R. Pless. Discrete and differential two-view constraints for general imaging system. In *IEEE Workshop on Omnidirectional Vision*, pages 53–59. IEEE Press, June 2002.

[14] H.-Y. Shum, A. Kalai, and S. M. Seitz. Omnivergent stereo. In *ICCV*, volume 1, pages 22–29, September 1999.

[15] H. Y. Shum, W. L., J. X. Chai, and T. X. Rendering by manifold hopping. *IJCV 50(2)*, pages 185–201, 2002.

[16] H. Y. Shum and R. Szeliski. Stereo Reconstruction from Multiperspective Panoramatas. In *ICCV*, volume 1, September 1999.

[17] J. Šivic and T. Pajdla. Geometry of concentric multiperspective panoramas. Research Report CTU–CMP–2002–05, Center for Machine Perception, 2002.

[18] P. Sturm. Mixing catadioptric and perspective cameras. In *Omnivis 2002*, pages 37–44.

[19] D. Weinshall, M.-S. Lee, T. Brodsky, M. Trajkovic, and D. Feldman. New view generation with a bi-centric camera. In *ECCV 2002*, pages 614–628.

[20] A. Zomet, D. Feldman, S. Peleg and D. Weinshall. Mosaicing New Views: The Crossed-Slits Projection. PAMI 25(6):741-754, June 2003.

[21] T. Werner and T. Pajdla. Cheirality in epipolar geometry. In *ICCV*, pages 548–553. IEEE Computer Society Press, July 2001.